Inorganic Chemistry
Article
Cite This: Inorg. Chem. XXXX, XXX, XXX−XXX
pubs.acs.org/IC

Successive and Specific Detection of Hg^{2+} and I^- by a DNA@MOF Biosensor: Experimental and Simulation Studies

Pei-Pei Hu,[†] Ning Liu,[†] Ke-Yang Wu,[†] Ling-Yan Zhai,[†] Bao-Ping Xie,[†] Bin Sun,[†] Wen-Jun Duan,[†] Wen-Hua Zhang,*[,‡] and Jin-Xiang Chen*[,†]

[†]Guangdong Provincial Key Laboratory of New Drug Screening, School of Pharmaceutical Sciences, Southern Medical University, Guangzhou 510515, China

[‡]College of Chemistry, Chemical Engineering and Materials Science, Soochow University, Suzhou 215123, China

Supporting Information

ABSTRACT: A 2D metal−organic framework (MOF) of $\{[Cu(Dcbb)(Bpe)]\cdot Cl\}_n$ (**1**, H_2DcbbBr = 1-(3,5-dicarboxybenzyl)-4,4′-bipyridinium bromide, Bpe = *trans*-1,2-bis(4-pyridyl)ethylene)) has been prepared. MOF **1** associates with the thymine-rich (T-rich), single-stranded probe DNA (ss-DNA, denoted as P-DNA) labeled with fluorophore FAM (FAM = carboxyfluorescein) and quenches the FAM emission to give a nonemissive P-DNA@**1** hybrid (off state). The P-DNA in the hybrid subsequently captures the Hg^{2+} to give a rigid double-stranded DNA featuring T−Hg^{2+}−T motif (ds-DNA@Hg^{2+}) and detach from MOF **1**, triggering the recovery of the FAM fluorescence (on state). Upon subsequent addition of I^-, Hg^{2+} was further sequestrated from the ds-DNA@Hg^{2+} duplex, driven by the stronger Hg−I coordination. The released P-DNA is resorbed by MOF **1** to regain the initial P-DNA@**1** hybrid (off state). The P-DNA@**1** sensor thus detects Hg^{2+} and I^- sequentially via a fluorescence "off−on−off" mechanism. The sensor is highly selective and sensitive, yielding detection limits of 3.2 and 3.3 nM, respectively. The detection process was conformed by circular dichroism (CD) and the detection mechanism was verified by fluorescence anisotropy, binding constant, and simulation of the binding free energy at each stage.

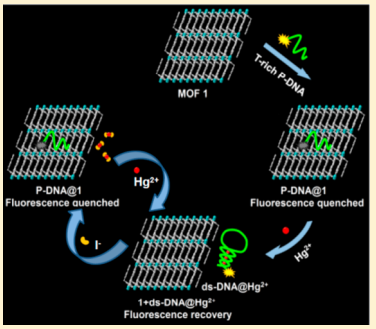

INTRODUCTION

Monitoring the level of notoriously toxic Hg^{2+} in water has a strong relevance to human health.[1] Hg^{2+} readily penetrates the skin in the respiratory tract and gastrointestinal tissue, leading to irreversible damage to the central nervous system and resulting in kidney failure as well as various cognitive and motion disorders, especially brain damage.[2] In addition, microbial biomethylation of Hg^{2+} yields methyl mercury which could pass through the placenta and is confined in the central nervous system, resulting in damage to the developing brain.[3] Since the Hg^{2+} in water is the major source of exposure and according to the World Health Organization (WHO), the maximum allowed Hg^{2+} concentration in drinking water is 30 nM.[4]

The other common yet biologically relevant anion is I^-. Consumption of I^- is crucial for thyroid hormone production.[5] However, excessive intake of I^- also results in hypothyroidism and hyperthyroidism, due to its cause of thyroid dysfunction.[6] Thyroid hormone deficiency during fetal and postnatal development causes retarded brain maturation, intellectual deficits, and neurological impairment in some cases.[7] In view of the impact of both Hg^{2+} and I^- on human brain development and the nervous system, it is imperative to monitor the Hg^{2+} and I^- levels in drinking water.

Metal−organic frameworks (MOFs) have appeared to be an attractive series of sensing materials for cations/anions, in addition to other promising properties related to porosity, material design capacity, and thermal/chemical stability.[8−14] The mostly practiced principle of metal ion detection by a MOF is that of decorating functional groups on its surface.[15,16] These functionalities include thiol,[17] pyridyl,[18] benzimidazolyl,[19] methionine,[20] and melamine,[21] which can specifically interact with metal ions, especially for Hg^{2+} due to its large ionic radius compared to most of the other metal ions.[22−27] The interaction between functional group and Hg^{2+} hinders the energy transfer from organic ligands to metals ions in MOFs and thus causes the luminescence decay of the MOFs.[28] In addition, the collapse of the MOF structures to regenerate the ligand by Hg^{2+} can also be used to selectively but irreversibly detect Hg^{2+}.[29] More recently, Zhang et al. pioneered the use of UiO-66-NH_2 for the construction of a P-DNA@MOF (P-DNA = probe DNA) hybrid system to selectively detect Hg^{2+} by forming hairpin-like thymine−Hg^{2+}−thymine (T−Hg^{2+}−T) structure.[30]

In sharp contrast, there are few reports on the use of MOFs for the detection of I^-.[31] Zhao et al. reported cationic heterometal−organic frameworks with NO_3^- in the channels, serving as highly sensitive and specific luminescent probe for I^- sensing in the aqueous phase through anion exchange.[32] More recently, Yang et al. incorporated Ag^{2+} into the framework of MIL-101 to elevate its intake of I^-.[33] Nonetheless, so far as we

Received: April 16, 2018

DOI: 10.1021/acs.inorgchem.8b01051
Inorg. Chem. XXXX, XXX, XXX−XXX

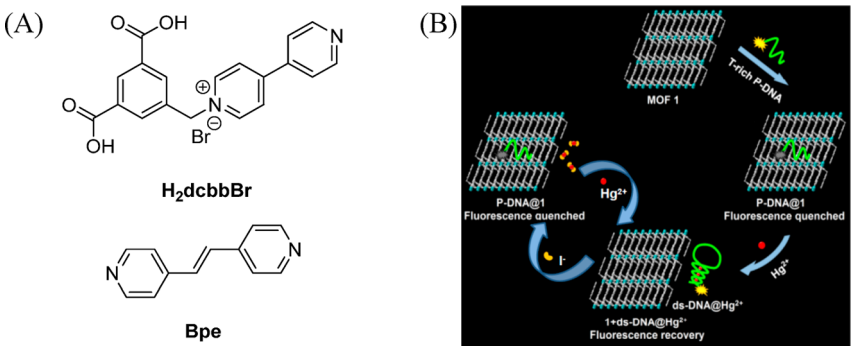

Figure 1. (A) Chemical structures of H_2DcbbBr and Bpe. (B) Detection mechanism of Hg^{2+} and I^- based on the hybrid of MOF **1** and T-rich P-DNA.

are aware, a biosensor based on P-DNA@MOF for I^-, as well as a sensing platform able to detect Hg^{2+} and I^- specifically in a one-pot process, has not been reported.

We herein report a biosensor composed from a 2D MOF of $\{[Cu(Dcbb)(Bpe)]\cdot Cl\}_n$ (**1**, H_2DcbbBr = 1-(3,5-dicarboxybenzyl)-4,4′-bipyridinium bromide, Bpe = *trans*-1,2-bis(4-pyridyl)ethylene, Figure 1A) and P-DNA, denoted as P-DNA@**1**, for the succession sensing of Hg^{2+} and I^-. As shown in Figure 1B, the emissive FAM-labeled (FAM = carboxyfluorescein) T-rich single-stranded probe DNA (ss-DNA, denoted as P-DNA, on state) can be absorbed on the surface of MOF **1** to form a P-DNA@**1** hybrid with fluorescence quenching (off state) through the PET (photoinduced electron transfer) process.[34−36] Upon introducing Hg^{2+}, each two N atoms from a pair of thymine bases (T) of the P-DNA strands coordinate to one Hg^{2+} to give a double-stranded DNA comprising hairpin-like T−Hg^{2+}−T subcomponent (ds-DNA@Hg^{2+}).[30] Upon Hg^{2+} association, the ds-DNA@Hg^{2+} also becomes more rigid compared to the random-coiled P-DNA and subsequently detaches from MOF **1** with the restoration of fluorescence (on state) and form **1** + ds-DNA@Hg^{2+}. With further addition of I^- into the **1** + ds-DNA@Hg^{2+} system, Hg^{2+} is extracted from the ds-DNA@Hg^{2+} due to the stronger affinity of I^- toward Hg^{2+}. As a consequence, the ds-DNA@Hg^{2+} unwinds to give P-DNA and resorbed by MOF **1**, accompanied by the quench of the fluorescence again (off state). Therefore, an "off−on−off" fluorescent sensing scenario with high sensitivity and specificity toward Hg^{2+} and I^- in succession has been achieved.

EXPERIMENTAL SECTION

The FT-IR spectra were collected on a Nicolet MagNa-IR 550 infrared spectrometer. Microanalysis data were collected on an EA1110 CHNS elemental analyzer. Powder X-ray diffraction (PXRD) date were collected on a Rigaku D/max2200/PC. The X-ray prompt from the sealed Cu tube was monochromated with a graphite crystal and collimated by a MONOCAP (0.5 mm, $\lambda_{CuK\alpha}$ = 1.54178 Å). The voltage and current of the tube were respectively set to 40 kV and 40 mA. Fluorescence spectra were measured on an LS 55 fluorescence spectrophotometer.

The H_2DcbbBr ligand was synthesized following our established procedure.[37] The thymine-rich probe DNA sequence (P-DNA: 5′-FAM-TTCTTCTTGCCCCCCTTGTTGTT-3′) were commercially available from Sangon Inc. (Shanghai, China) and were dissolved in Hepes buffer (pH 7.4, 20 mM, Hepes = 2-[4-(2-hydroxyethyl)-1-piperazinyl] ethanesulfonic acid). These samples were respectively stored at −20 and −80 °C for immediate use and long-term preservation. All the other chemicals were directly from commercial sources and used as received.

Synthesis of $\{[Cu(Dcbb)(Bpe)]\cdot Cl\}_n$ (1). Powder of H_2DcbbBr (166.0 mg, 0.4 mmol) was dispersed in H_2O (20 mL) by sonication. The pH was adjusted to 7.0 using NaOH (0.1 M) to give a clear solution. This is followed by dropwise addition of $CuCl_2$ (26.9 mg, 0.2 mmol) dissolved in H_2O (20 mL). The mixture was further stirred for 30 min to give a homogeneous blue solution. Subsequently, Bpe (36 mg, 0.2 mmol) dissolved in DMF (1 mL) was slowly added, and the mixture was shaken for a while to give a blue solution containing a small amount of blue precipitate. After filtration, the filtrate was kept at room temperature for several days to obtain crystals of MOF **1**, which was collected by filtration and washed with diethyl ether and dried in vacuo (104.9 mg, 85%). Anal. Calcd (%) for $C_{31}H_{23}ClCuN_4O_4$: C 60.59, H 3.77, N 9.12. Found: C 60.21, H 4.19, N 8.58. IR (KBr disc, cm^{-1}) ν 3556 (s), 3279 (m), 1640 (m), 1626 (s), 1573 (s), 1412 (m), 1372 (m), 829 (m), 782 (m), 722 (m), 621 (m), 479 (m).

Single-Crystal X-ray Crystallography. Single-crystal X-ray crystallographic study for MOF **1** was carried out on a Bruker APEX II diffractometer coupled with graphite-monochromated Mo Kα (λ = 0.71073 Å) irradiation. The data were corrected and absorption correction with SADABS subsequently performed.[38] The structure was solved by direct method and refined by full-matrix least-squares techniques on F^2 with SHELXTL-2013 program.[39] While acceptable solvent model could not be achieved for some spatially delocalized electron density in the lattice, such solvent contribution was then modeled with SQUEEZE function in the Platon suite.[40,41] The data of MOF **1** have been deposited in the CCDC (Cambridge Crystallographic Data Center) with number of 1845959. These data can be either downloaded free of charge from the CCDC via www.ccdc.cam.ac.uk/data_request/cif or from the Supporting Information. Some relevant crystallographic data and bond parameters for MOF **1** are listed in Tables S1 and S2.

Hg^{2+} and I^- Detection Experiments. All the experiments described below were carried out in 20 mM Hepes buffer (pH 7.4) at room temperature. The fluorescence intensity at 518 nm (λ_{ex} = 480 nm) was used for quantitative analysis, with both excitation and emission slit widths set to 10.0 nm. Each experiment was repeated three times with their average values used for calculation.

Step 1: Establishment of the Hg^{2+} Sensor. A solution of P-DNA (50 nM) was stirred with various concentrations of MOF **1** containing 50 nM P-DNA until quenching is saturated to form a P-DNA@**1** hybrid (Hg^{2+} sensor). The emission data were measured accordingly and the quenching efficiency (Q_E, %) deduced from eq 1.

$$Q_E = (1 - F_M/F_0) \times 100\% \quad (1)$$

wherein F_M/F_0 features fluorescent intensities at 518 nm in the presence/absence of MOF **1**.

Step 2: Evaluation of the Detection Sensitivity of the Hg^{2+} Sensor and Construction of the I^- Sensor. Hg^{2+} of varied concentrations were introduced into the P-DNA@**1** solution, followed by incubation for 30 min to give the **1** + ds-DNA@Hg^{2+} system (I^- sensor), and eq 2 was used for the deduction of the fluorescence recovery efficiency (R_E).

DOI: 10.1021/acs.inorgchem.8b01051
Inorg. Chem. XXXX, XXX, XXX−XXX

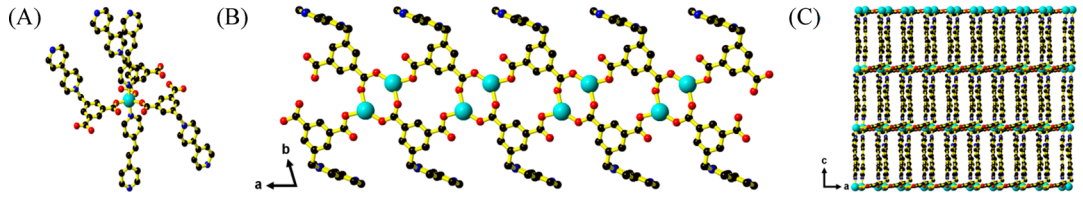

Figure 2. Structure of MOF **1**. (A) Full coordination sphere of the Cu^{2+}. (B) 1D chain defined by Cu^{2+} and Dcbb ligand propagating along the *a* axis. (C) 2D structure extended within the *ac* plane. Color legend: Cu (cyan), O (red), N (blue), and C (black).

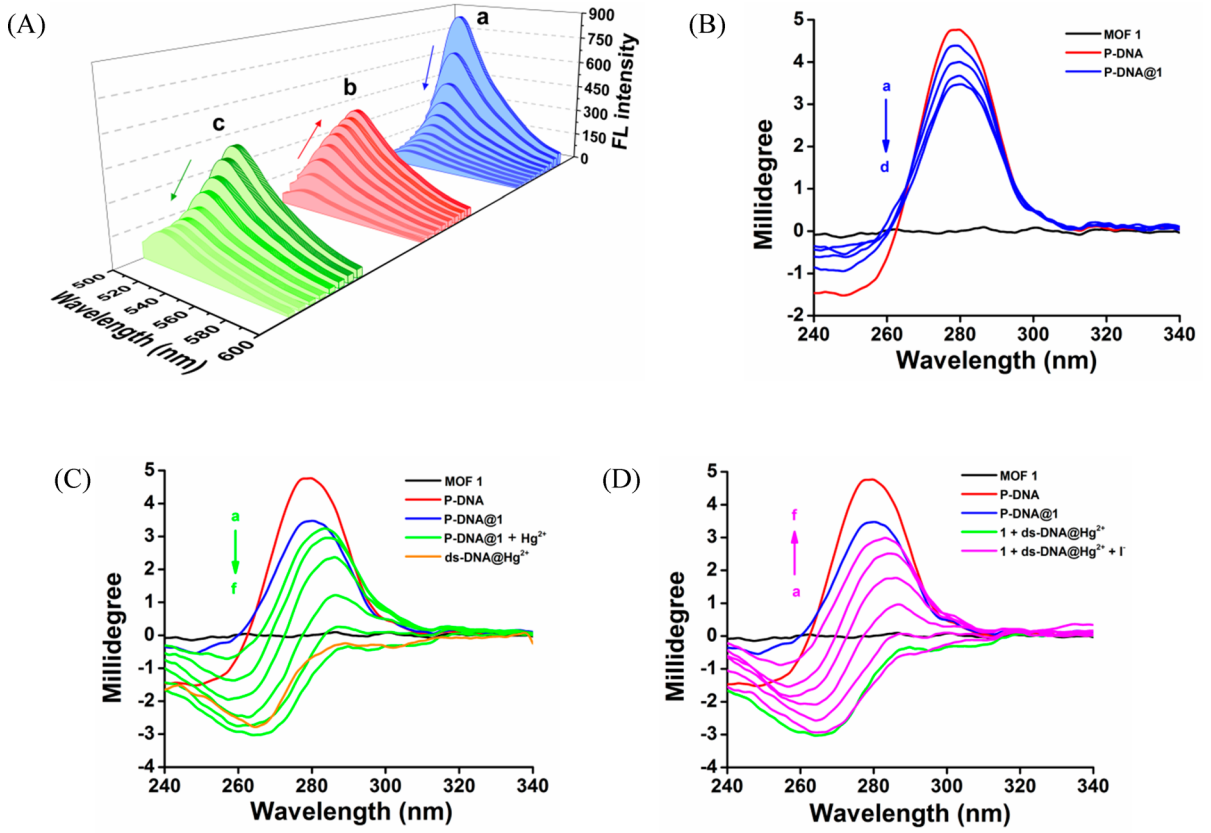

Figure 3. (A) Emission quenching of P-DNA (50 nM) incubated with different concentrations of MOF **1** (a), emission recovery of P-DNA@**1** (50 nM/12 μM) sensing system toward different concentrations of Hg^{2+} (b), and fluorescence quenching of **1** + ds-DNA@Hg^{2+} (12 μM/50 nM/1 μM) sensing system toward different concentrations of I^- (c). (B) CD spectra of MOF **1** (250 μM) and P-DNA (10 μM) with different concentrations of MOF **1** (50, 83, 107, and 125 μM, a–d). (C) CD spectra of P-DNA@**1** (10 μM/125 μM) with different concentrations of Hg^{2+} (15, 22.5, 30, 37.5, 45, and 52.5 μM, a–f) and ds-DNA@Hg^{2+} (10 μM/52.5 μM). (D) CD spectra of **1** + ds-DNA@Hg^{2+} (125 μM/10 μM/52.5 μM) with different concentrations of I^- (30, 45, 60, 75, 90, and 105 μM, a–f).

$$R_E = F_T/F_M - 1 \quad (2)$$

wherein F_T/F_M represents the emission intensity at 518 nm in the presence/absence of Hg^{2+}.

Step 3: Assessment of the Detection Sensitivity of the I^- Sensor. Adding I^- of varied concentrations to the above **1** + ds-DNA@Hg^{2+} solution until quenching was saturated and the Q_E calculated according to eq 1.

To evaluate the selectivity and sensitivity of the Hg^{2+} and I^- sensors, other metal cations, including Ba^{2+}, Ca^{2+}, Cd^{2+}, Cu^{2+}, K^+, Mg^{2+}, Mn^{2+}, Na^+, Ni^{2+}, and Pb^{2+}, as well as the anions, including SO_4^{2-}, CO_3^{2-}, NO_3^-, OH^-, HSO_4^-, $H_2PO_4^-$, F^-, Cl^-, and Br^-, with concentrations 10-fold higher than those of Hg^{2+} and I^- were investigated under the same experimental conditions.

The emission intensity changes of P-DNA and ds-DNA@Hg^{2+} at the emission wavelength of 518 nm were invoked to estimate their binding constant (K_b) and binding stoichiometry (n) for their association with MOF **1** following eq 3.

$$\mathrm{Log}[(F_0 - F)/F] = n\,\mathrm{Log}[Q] + \mathrm{Log}\,K_b \quad (3)$$

wherein F_0/F represents the emission intensities in the absence/presence of different concentrations of MOF **1**, and [*Q*] is the concentration of MOF **1**.

Molecular Simulation Studies. MOF **1** with 2D structure, P-DNA, and ds-DNA@Hg^{2+} with chain structures were constructed using Molecular Operating Environment (MOE) package.[42] The initial structure of P-DNA@**1** or **1** + ds-DNA@Hg^{2+} was manually built by placement of P-DNA or ds-DNA@Hg^{2+} in the location 2 Å to the MOF **1** plane. Structures were first optimized in MOE using MMFF94x force field and then reoptimized in UFF of Gaussian 09[43] where Gibbs free energy calculations were simplified by calculating single point energies. Finally, Python molecule (PyMOL)[44] was employed for visual analysis of binding modes. The binding free energy difference ($\Delta\Delta G$) between reactions of MOF **1** with single chain P-DNA ($\Delta G_{\text{P-DNA@MOF}}$) or double chain ds-DNA@Hg^{2+} ($\Delta G_{\text{MOF+ds-DNA@Hg}^{2+}}$) is evaluated according to the following:

DOI: 10.1021/acs.inorgchem.8b01051
Inorg. Chem. XXXX, XXX, XXX–XXX

$$\Delta\Delta G = \Delta G_{\text{P-DNA@MOF}} - \Delta G_{\text{MOF+ds-DNA@Hg}^{2+}}$$
$$= [G_{\text{P-DNA@MOF}} - (G_{\text{MOF}} + G_{\text{P-DNA}}) - [G_{\text{MOF+ds-DNA@Hg}^{2+}} - (G_{\text{MOF}} + G_{\text{ds-DNA@Hg}^{2+}})]$$
$$= (G_{\text{P-DNA@MOF}} - G_{\text{MOF+ds-DNA@Hg}^{2+}}] - (G_{\text{P-DNA}} - G_{\text{ds-DNA@Hg}^{2+}}) \quad (4)$$

RESULTS AND DISCUSSION

Synthesis and Characterization of MOF 1. MOF **1** was prepared in 85% yield by reacting $CuCl_2$ with deprotonated zwitterionic carboxylate H_2DcbbBr and Bpe. Powder of MOF **1** was placed in Hepes buffer (pH 7.4, 20 mM) at room temperature and sonicated to yield a suspension. The suspension was kept for 12 h and then isolated by centrifugation. The precipitate collected was dried in vacuum. The powder X-ray diffraction (PXRD) pattern of the recollected sample of **1** is agreeable with that simulated from the crystallographic data, both indicating its phase purity and biological system stability (Figure S1).

Crystal Structure of $\{[Cu(Dcbb)(Bpe)]\cdot Cl\}_n$ (1). MOF **1** crystallizes in triclinic space group $P\bar{1}$ with its asymmetric unit features one [Cu(Dcbb)(Bpe)] molecule and one Cl^- anion. Each Cu^{2+} is bonded with two N atoms of a pair of Bpe molecules, two O atoms from a pair of bridging carboxylates (μ_2-η^1, η^1), and one monodentate carboxylate from the third Dcbb ligand, yielding a trigonal bipyramidal coordination geometry for each Cu^{2+} (Figure 2A). A pair of μ-carboxylates juxtaposes two Cu^{2+} to give a dimeric unit of $[Cu_2(Dcbb)_2]$. Such a dimer extends to 2 equiv to form a 1D chain propagating in the *a* axis (Figure 2B). Adjacent 1D chains are approximately 11.1 Å apart. This distance approximates the length of a Bpe ligand (ca. 7.08 Å) plus two Cu−N bonds (ca. 2.0 Å for each). Thus, the Bpe ligands are snuggly accommodated, and the Cu−Bpe chain is aligned in the *c* direction to result in a 2D network in *ac* plane (Figure 2C).

Sensing Properties of MOF 1 toward Hg^{2+} and I^-. We conducted all the detection process in Hepes buffer (pH 6.8−8.2) as it showed higher detection sensitivity and selectivity than in Tris-HCl (pH 7.1−9.0) and MOPS (MOPS = 3-(*N*-morpholino)propanesulfonic acid, pH 6.5−7.9). The construction of P-DNA@**1** hybrid system (Hg^{2+} sensor) is based on the affinity between MOF **1** and P-DNA, which has been demonstrated in our previous studies.[45−49] In order to verify the detection sensitivity of Hg^{2+} and I^-, we conducted the following experiments. In the first step, we established the optimal Hg^{2+} sensor by mixing MOF **1** and T-rich P-DNA (50 nM) in Hepes buffer (pH 7.4, 20 mM). As shown in Figures 3A-a and S2a, with the addition of MOF **1**, the emission intensity of P-DNA decreased continuously until saturation, and the Q_E of 90.5% was achieved with the concentration of 12 μM for MOF **1**. This concentration was selected for the following experiments as it provides the lowest background emission for the detection of Hg^{2+}.

In the second step, we evaluated the detection sensitivity of the P-DNA@**1** sensor toward Hg^{2+}. As shown in Figures 3A-b and S2b, when incubating different concentrations of Hg^{2+} with P-DNA@**1** hybrid, the fluorescence intensity was significantly recovered until saturation (1 μM Hg^{2+}) observed with the recovery efficiency (R_E) being 3.9. The fluorescence recovery is observed due to the strong bonding between the Hg^{2+} and the N atoms of the T bases to form the rigid hairpin-like T−Hg−T duplex ds-DNA@Hg^{2+}, which is subsequently repelled by MOF **1**.[50] The **1** + ds-DNA@Hg^{2+} system thus formed in turn functions as the I^- sensor. The limit of detection (LOD) for Hg^{2+} was calculated as 3.2 nM based on 3σ/slope (σ = standard deviation for 10 blank samples), which is nearly an order of magnitude lower than the maximum allowable Hg^{2+} concentration in drinking water (30 nM) defined by the WHO.[4] The recoveries of mercury ions in serum and environmental water samples were from 94.6 to 99.1% (Table S3).

The final step is to assess the detection sensitivity of the constructed I^- sensor of **1** + ds-DNA@Hg^{2+}. Comparing the formation constant of HgI_2 (8.3×10^{23} M^{-1})/HgI_4^{2-} (5.6×10^{29} M^{-1}) with T−Hg−T (10^6 M^{-1}), it is obvious that Hg^{2+} exhibits a much higher affinity for I^- than the T base. Thus, I^- will sequester the Hg^{2+} from ds-DNA@Hg^{2+} to give HgI_2/HgI_4^{2-}.[51] The unwound P-DNA is subsequently resorbed by MOF **1**, leading to the fluorescence quenching again. As illustrated in Figures 3A-c and S2c, upon adding different concentrations of I^- to the **1** + ds-DNA@Hg^{2+} system, the fluorescence intensity decreased with an increased concentration of I^- from 0 to 2 μM. The Q_E and the LOD were calculated to be 64.7% and 3.3 nM, respectively. Such LOD is comparable to that of $\{Tb_2Zn(L)_3(H_2O)_4](NO_3)_2\cdot 12H_2O\}_n$ (L = 4,4′-dicarboxylate-2,2′-dipyridine anion) (10 nM) reported by Zhao et al.[32] The recoveries of I^- in serum and environmental water samples were from 94.1 to 104.6% (Table S3). The Hg^{2+} and I^- detection process can be repeated three times with the effective R_E values for Hg^{2+} and Q_E values for I^- (Table S4), indicating the stability of the sensor.

In order to further elaborate the detection process, the P-DNA conformation change caused by Hg^{2+} and I^- was studied by circular dichroism (CD) spectroscopy. Single-stranded P-DNA with a concentration of 10 μM respectively exhibited a positive CD peak. The intensity of the peak gradually decreased with the increased concentrations of MOF **1** (Figure 3B). MOF **1** fails to absorb all the P-DNA (10 μM) at its highest concentration of 250 μM, leading to partial disappearance of the CD peak only. With an increased concentration of Hg^{2+} in the P-DNA@**1** sensing system, the intensity of positive peak weakened and ultimately disappeared, accompanied by the continuously increased intensity of the negative peak with also slight redshift (Figure 3C), attributable to the formation of a large amount of T−Hg^{2+}−T ds-DNA@Hg^{2+}complex.[50] Finally, with the addition of I^- to the **1** + ds-DNA@Hg^{2+} system, the negative peak disappeared and the positive peak appeared again, indicating that the ds-DNA@Hg^{2+} (T−Hg^{2+}−T) unwind to release P-DNA (Figure 3D). In Figure 3D, the CD signal upon regeneration of P-DNA does not completely reach its initial millidegree (the blue one), likely ascribed to the existence of equilibrium of the ds-DNA@Hg^{2+} and HgI_2/HgI_4^{2-} in the solution and the release of P-DNA is not complete.

The above observations are ascribed to the structural features of MOF **1**. First, MOF **1** is sustained by a zwitterionic ligand featuring aromatic rings and positively charged pyridinium centers. This unique ligand further lined up with positively charged Cu^{2+} to yield a 2D sheet structure with high surface exposure. MOF **1** is thus able to associate with the P-DNA through a variety of intermolecular forces, such as electrostatic, π-stacking, and/or hydrogen-bonding, to give a P-DNA@**1** hybrid with quenched FAM emission.[34−36] Second,

DOI: 10.1021/acs.inorgchem.8b01051
Inorg. Chem. XXXX, XXX, XXX−XXX

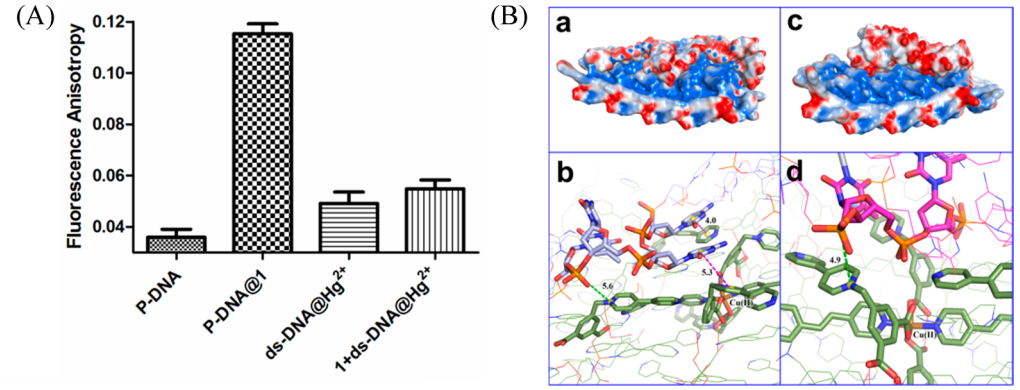

Figure 4. (A) Changes of fluorescence anisotropy of P-DNA (50 nM) and ds-DNA@Hg^{2+} (50 nM/1 μM) prior and after the addition of MOF **1** (12 μM). (B) Interactions between MOF **1** and P-DNA and ds-DNA@Hg^{2+}: (a) and (c) charge distributions where red area represented negative charges, blue positive, and white neutral; (b) and (d) local binding modes where MOF **1** was displayed by smudge lines and sticks, while P-DNA by light blue lines and sticks. Charge centers and aromatic ring centers were denoted by yellow spheres, $\pi-\pi$ stacking interactions by magenta dashes, and salt bridges by green dashes.

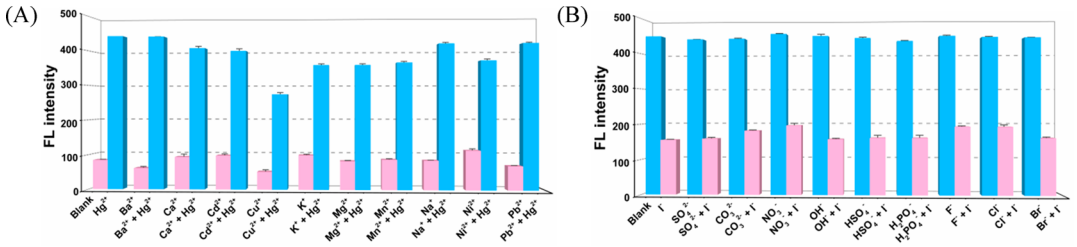

Figure 5. (A) Detection selectivity of Hg^{2+} sensor (blank: P-DNA@**1** (50 nM/12 μM); Hg^{2+}: 1 μM, other metal ions: 10 μM). (B) Detection selectivity of I^- sensor (blank: **1** + ds-DNA@Hg^{2+} (12 μM/50 nM/1 μM); I^-: 2 μM, other anions: 20 μM).

in the subsequent emission recovery step, MOF **1** plays a vital role in distinguishing single-stranded P-DNA (ss-P-DNA) from the ds-DNA@Hg^{2+} duplex.[46] Due to the absence of unpaired bases, the relatively rigid structures, and the large cross-sectional areas, the formed ds-DNA@Hg^{2+} duplex fails to effectively interact with MOF **1**. In sharp contrast, the P-DNA with conformational flexibility and smaller cross-sectional area should be able to "induced fit" to interact with MOF **1** via multiple noncovalent interactions.[49] Therefore, the coordination of Hg^{2+} with the absorbed P-DNA would trigger the release of the latter from MOF **1** to give the duplex of ds-DNA@Hg^{2+}, leading to the emission recovery. Such assumption is further evidenced by the alteration of the fluorescence anisotropy (FA) of the P-DNA and ds-DNA@Hg^{2+} (hybrid duplex) prior and after the introduction of MOF **1**, respectively. It is established that when a fluorophore is bound to a molecule, e.g., FAM to ss-DNA, to give P-DNA in the present case, the motion-related factors increase when the P-DNA was adsorbed by MOF **1** due to its large molecular size.[46] Thus, FA functions as a means to estimate if P-DNA or ds-DNA@Hg^{2+} is associated with the surface of MOF **1**. As shown in Figure 4A, the addition of MOF **1** into the P-DNA led to an increase in the FA by factors from 0.036 ± 0.003 to 0.115 ± 0.004, whereas negligible influence was observed for ds-DNA@Hg^{2+}. These results suggest the stronger interaction of MOF **1** with the P-DNA than with hybrid duplex ds-DNA@Hg^{2+}. The binding constants of MOF **1** with P-DNA (2.58×10^5 M^{-1}) is 14 times higher than that with ds-DNA@Hg^{2+} (1.9×10^4 M^{-1}), further suggesting stronger association of MOF **1** with P-DNA than with ds-DNA@Hg^{2+} duplex.

To further elucidate the detection mechanism, the binding free energy difference ($\Delta\Delta G$) between reactions of MOF **1** with P-DNA ($\Delta G_{\text{P-DNA@MOF}}$) and MOF **1** with ds-DNA@Hg^{2+} ($\Delta G_{\text{MOF+ds-DNA@Hg}^{2+}}$) is calculated. When $\Delta\Delta G < 0$ ($\Delta G_{\text{P-DNA@MOF}} < \Delta G_{\text{MOF+ds-DNA@Hg}^{2+}}$), meaning that the binding of P-DNA to MOF **1** is stronger than that of ds-DNA@Hg^{2+} and vice versa. Gibbs free energy calculations were simplified by calculating single point energies. The result (Table S5) showed that $\Delta\Delta G = -83.38$ kcal/mol < 0, suggesting that P-DNA bounds to MOF **1** more tightly than ds-DNA@Hg^{2+}, in accordance with the experimental observation.

The electrostatic surface showed that the surface of MOF **1** was largely positive and P-DNA was covered by a negative and neutral surface with the scattered positive area, which led to good electronic complement between MOF **1** and P-DNA. Single chain P-DNA exhibits higher contact area with MOF **1** due to its structural flexibility, while double chain ds-DNA@Hg^{2+} only has a small interface (Figure 4B-a,B-c). P-DNA bound to MOF **1** mainly by $\pi-\pi$ stacking of aromatic rings and salt bridges between phosphate groups and pyridinium moieties. Figure 4B-b displayed two $\pi-\pi$ stacking between cytosine and bipyridinium with distances between ring centroid of 4.0−5.3 Å, in addition to a salt bridge with charge center distances of 5.6 Å. In stark contrast, the ds-DNA@Hg^{2+} interacted with MOF **1** primarily through a small number of salt bridges (4.9 Å) between the phosphate group and the pyridinium N^+ center (Figure 4B-d).

The specificity of the Hg^{2+} sensor was assessed by comparing its response to Hg^{2+} and those contaminated with other metal cations including Ba^{2+}, Ca^{2+}, Cd^{2+}, Cu^{2+}, K^+, Mg^{2+},

DOI: 10.1021/acs.inorgchem.8b01051
Inorg. Chem. XXXX, XXX, XXX−XXX

Mn^{2+}, Na^{+}, Ni^{2+}, and Pb^{2+}. There exists limited fluorescence intensity change caused by other metal cations (10 μM), whereas the emission intensity enhanced significantly upon introducing Hg^{2+} (1 μM) (Figure 5A). Subsequently, Hg^{2+} (1 μM) was added to the solution of other metal ions (10 μM), leading to the large fluorescence intensity enhancement and suggesting that the present sensor detects Hg^{2+} with high sensitivity and selectivity. Similarly, we also compared detection specificity of the sensor to I^- and other small anions, such as SO_4^{2-}, CO_3^{2-}, NO_3^-, OH^-, HSO_4^-, $H_2PO_4^-$, F^-, Cl^-, and Br^-. As depicted in Figure 5B, the fluorescence intensity induced by the other anions (20 μM, 10-fold higher than I^-) only showed a negligible response to fluorescence quenching. While for I^- (2 μM) or I^- (2 μM) mixed with other small anions, it gained a significant fluorescence decrease, indicating that the sensor possesses sensitivity and selectivity toward I^-.

CONCLUSION

We have developed for the first time a sensing system based on the P-DNA@MOF hybrid that is able to sensitively and specifically detect Hg^{2+} and I^- in succession in one pot. With Cu-based MOF **1**, coupled with thymine-pertaining P-DNA well-known to support hairpin-like T−Hg−T duplex, we achieved a Hg^{2+} detection limit of 3.2 nM which is 1 order of magnitude lower than that allowable in drinking water. The strong affinity of Hg^{2+} toward I^- also inspired us to directly adopt the Hg^{2+}-sensing product for I^-, giving a low I^- detection limit of 3.3 nM, thus completes a dual sensing of two biologically relevant ions. The integration of MOF, chromophore-tagged DNA sequences, and simple competitive coordination chemistry may allow the one-pot dual sensing of other biorelevant cations (such as Pb^{2+}, Cu^{2+}, and Fe^{3+}) and anions (such as PO_4^{3-}, Cl^-, and S^{2-}) to be executed with high sensitivity and selectivity, and we are currently exploring such systems.

ASSOCIATED CONTENT

Supporting Information

The Supporting Information is available free of charge on the ACS Publications website at DOI: 10.1021/acs.inorgchem.8b01051.

Crystallographic data; selected bond distances; determination of Hg^{2+} in serum and environmental water (n = 3); the recycle detection for Hg^{2+} (R_E) and I^- (Q_E); the electronic energies calculated in UFF force field; the simulated and experimental PXRD patterns of MOF **1**; the emission quenching of the P-DNA (50 nM) upon incubating with MOF **1** of various concentrations; the emission recovery of P-DNA@**1** (50 nM/12 μM) sensing system toward Hg^{2+} with different concentrations; the fluorescence quenching of **1** + ds-DNA@Hg^{2+} (12 μM/50 nM/1 μM) sensing system toward I^- with different concentrations (PDF)

Accession Codes

CCDC 1845959 contains the supplementary crystallographic data for this paper. These data can be obtained free of charge via www.ccdc.cam.ac.uk/data_request/cif, or by emailing data_request@ccdc.cam.ac.uk, or by contacting The Cambridge Crystallographic Data Centre, 12 Union Road, Cambridge CB2 1EZ, UK; fax: +44 1223 336033.

AUTHOR INFORMATION

Corresponding Authors

*E-mail: jxchen@smu.edu.cn.

*E-mail: whzhang@suda.edu.cn.

ORCID

Wen-Hua Zhang: 0000-0001-9047-8881

Jin-Xiang Chen: 0000-0002-3963-0718

Notes

The authors declare no competing financial interest.

ACKNOWLEDGMENTS

We acknowledge the financial support from the Guangdong Provincial Natural Science Foundation of China (2015A030313284), Guangdong Provincial Department of Science and Technology of China (2015A010105016), the National Natural Science Foundation of China (21671143), and Southern Medical University. We are also grateful to Dr. Ziying Zhang from Guangzhou Yinfo Information Technology Co., Ltd. for the molecular simulation studies.

REFERENCES

(1) Renzoni, A.; Zino, F.; Franchi, E. Mercury levels along the food chain and risk for exposed populations. *Environ. Res.* **1998**, *77*, 68−72.

(2) Grandjean, P.; Weihe, P.; White, R. F.; Debes, F. Cognitive performance of children prenatally exposed to "safe" levels of methylmercury. *Environ. Res.* **1998**, *77*, 165−172.

(3) Trasande, L.; Landrigan, P. J.; Schechter, C. Public health and economic consequences of methyl mercury toxicity to the developing brain. *Environ. Health Perspect.* **2005**, *113*, 590−596.

(4) Zhang, L.; Li, T.; Li, B.; Li, J.; Wang, E. Carbon nanotube-DNA hybrid fluorescent sensor for sensitive and selective detection of mercury(II) ion. *Chem. Commun.* **2010**, *46*, 1476−1478.

(5) Chen, Z.; Niu, Y.; Cheng, G.; Tong, L.; Zhang, G.; Cai, F.; Chen, T.; Liu, B.; Tang, B. A fast, highly sensitive and selective assay of iodide ions with single-stranded DNA-templated copper nanoparticles as a fluorescent probe for its application in Kunming mice samples. *Analyst* **2017**, *142*, 2781−2785.

(6) Leung, A. M. *The effects of iodine excess*; Springer International Publishing AG, 2017; pp 75−89.

(7) Bernal, J. Thyroid hormone receptors in brain development and function. *Nat. Clin. Pract. Endocrinol. Metab.* **2007**, *3*, 249−259.

(8) Lin, Y.; Zhang, Q.; Zhao, C.; Li, H.; Kong, C.; Shen, C.; Chen, L. An exceptionally stable functionalized metal-organic framework for lithium storage. *Chem. Commun.* **2015**, *51*, 697−699.

(9) Wang, Q.; Bai, J.; Lu, Z.; Pan, Y.; You, X. Finely tuning MOFs towards high-performance post-combustion CO_2 capture materials. *Chem. Commun.* **2016**, *52*, 443−452.

(10) Kreno, L. E.; Leong, K.; Farha, O. K.; Allendorf, M.; Van Duyne, R. P.; Hupp, J. T. Metal-organic framework materials as chemical sensors. *Chem. Rev.* **2012**, *112*, 1105−1125.

(11) Furukawa, H.; Cordova, K. E.; O'Keeffe, M.; Yaghi, O. M. The chemistry and applications of metal-organic frameworks. *Science* **2013**, *341*, 1230444.

(12) Liu, D.; Ren, Z. G.; Li, H. X.; Lang, J. P.; Li, N. Y.; Abrahams, B. F. Single-crystal-to-single-crystal transformations of two three-dimensional coordination polymers through regioselective [2 + 2] photodimerization reactions. *Angew. Chem., Int. Ed.* **2010**, *49*, 4767−4770.

(13) Liu, D.; Lang, J. P.; Abrahams, B. F. Highly efficient separation of a solid mixture of naphthalene and anthracene by a reusable porous metal-organic framework through a single-crystal-to-single-crystal transformation. *J. Am. Chem. Soc.* **2011**, *133*, 11042−11045.

(14) Li, Y. A.; Yang, S.; Li, Q. Y.; Ma, J. P.; Zhang, S.; Dong, Y. B. UiO-68-ol NMOF-based fluorescent sensor for selective detection of HClO and its application in bioimaging. *Inorg. Chem.* **2017**, *56*, 13241−13248.

DOI: 10.1021/acs.inorgchem.8b01051
Inorg. Chem. XXXX, XXX, XXX−XXX

(15) Gu, T. Y.; Dai, M.; Young, D. J.; Ren, Z. G.; Lang, J. P. Luminescent Zn (II) coordination polymers for highly selective sensing of Cr (III) and Cr (VI) in water. *Inorg. Chem.* **2017**, *56*, 4668−4678.
(16) Hu, F. L.; Shi, Y. X.; Chen, H. H.; Lang, J. P. A Zn (II) coordination polymer and its photocycloaddition product: syntheses, structures, selective luminescence sensing of iron (III) ions and selective absorption of dyes. *Dalton Trans.* **2015**, *44*, 18795−18803.
(17) Yee, K. K.; Reimer, N.; Liu, J.; Cheng, S. Y.; Yiu, S. M.; Weber, J.; Stock, N.; Xu, Z. Effective mercury sorption by thiol-laced metal-organic frameworks: in strong acid and the vapor phase. *J. Am. Chem. Soc.* **2013**, *135*, 7795−7798.
(18) Yang, J.; Wang, Z.; Li, Y. S.; Zhuang, Q. X.; Zhao, W. R.; Gu, J. L. Porphyrinic MOFs for reversible fluorescent and colorimetric sensing of mercury(II) ions in aqueous phase. *RSC Adv.* **2016**, *6*, 69807−69814.
(19) Xu, F.; Kou, L.; Jia, J.; Hou, X.; Long, Z.; Wang, S. Metal-organic frameworks of zeolitic imidazolate framework-7 and zeolitic imidazolate framework-60 for fast mercury and methylmercury speciation analysis. *Anal. Chim. Acta* **2013**, *804*, 240−245.
(20) Mon, M.; Lloret, F.; Ferrando-Soria, J.; Marti-Gastaldo, C.; Armentano, D.; Pardo, E. Selective and efficient removal of mercury from aqueous media with the highly flexible arms of a bioMOF. *Angew. Chem., Int. Ed.* **2016**, *55*, 11167−11172.
(21) Xia, T.; Song, T.; Zhang, G.; Cui, Y.; Yang, Y.; Wang, Z.; Qian, G. A terbium metal-organic framework for highly selective and sensitive luminescence sensing of Hg^{2+} ions in aqueous solution. *Chem. - Eur. J.* **2016**, *22*, 18429−18434.
(22) Zhu, Y. P.; Ma, T. Y.; Ren, T. Z.; Yuan, Z. Y. Mesoporous cerium phosphonate nanostructured hybrid spheres as label-free Hg^{2+} fluorescent probes. *ACS Appl. Mater. Interfaces* **2014**, *6*, 16344−16351.
(23) Liu, M.; Li, G.; Cheng, Z. A novel dual-functional fluorescent chemosensor for the selective detection of 2, 4, 6-trinitrotoluene and Hg^{2+}. *New J. Chem.* **2015**, *39*, 8484−8491.
(24) Xavier, S. S. J.; Siva, G.; Annaraj, J.; Kim, A. R.; Yoo, D. J.; kumar, G. G. Sensitive and selective turn-off-on fluorescence detection of Hg^{2+} and cysteine using nitrogen doped carbon nanodots derived from citron and urine. *Sens. Actuators, B* **2018**, *259*, 1133−1143.
(25) Li, W. X.; Li, H. X.; Li, H. Y.; Chen, M. M.; Shi, Y. X.; Lang, J. P. 1, 4-Bis (2-(pyridin-4-yl) vinyl) naphthalene and its zinc (II) coordination polymers: synthesis, structural characterization, and selective luminescent sensing of mercury (II) ion. *Cryst. Growth Des.* **2017**, *17*, 3948−3959.
(26) Gong, W. J.; Ren, Z. G.; Li, H. X.; Zhang, J. G.; Lang, J. P. Cadmium (II) coordination polymers of 4-pyr-poly-2-ene and carboxylates: construction, structure, and photochemical double [2 + 2] cycloaddition and luminescent sensing of nitroaromatics and mercury (II) ions. *Cryst. Growth Des.* **2017**, *17*, 870−881.
(27) Gong, W. J.; Yao, R.; Li, H. X.; Ren, Z. G.; Zhang, J. G.; Lang, J. P. Luminescent cadmium (ii) coordination polymers of 1, 2, 4, 5-tetrakis (4-pyridylvinyl) benzene used as efficient multi-responsive sensors for toxic metal ions in water. *Dalton Trans.* **2017**, *46*, 16861−16871.
(28) Dorazco-Gonzalez, A.; Alamo, M. F.; Godoy-Alcantar, C.; Hopfl, H.; Yatsimirsky, A. K. Fluorescent anion sensing by bisquinolinium pyridine-2,6-dicarboxamide receptors in water. *RSC Adv.* **2014**, *4*, 455−466.
(29) Wu, P.; Liu, Y.; Liu, Y.; Wang, J.; Li, Y.; Liu, W.; Wang, J. Cadmium-based metal-organic framework as a highly selective and sensitive ratiometric luminescent sensor for mercury(II). *Inorg. Chem.* **2015**, *54*, 11046−11048.
(30) Wu, L. L.; Wang, Z.; Zhao, S. N.; Meng, X.; Song, X. Z.; Feng, J.; Song, S. Y.; Zhang, H. J. A metal-organic framework/DNA hybrid system as a novel fluorescent biosensor for mercury(II) ion detection. *Chem. - Eur. J.* **2016**, *22*, 477−480.
(31) Lang, J. P.; Xu, Q. F.; Yuan, R. X.; Abrahams, B. F. $\{[WS_4Cu_4(4,4'\text{-bpy})_4][WS_4Cu_4I_4(4,4'\text{- bpy})_2]\}_\infty$-an unusual 3D porous coordination polymer formed from the preformed cluster $[Et_4N]_4[WS_4Cu_4I_6]$. *Angew. Chem., Int. Ed.* **2004**, *43*, 4741−4745.
(32) Shi, P. F.; Hu, H. C.; Zhang, Z. Y.; Xiong, G.; Zhao, B. Heterometal-organic frameworks as highly sensitive and highly selective luminescent probes to detect I^- ions in aqueous solutions. *Chem. Commun.* **2015**, *51*, 3985−3988.
(33) Mao, P.; Qi, B.; Liu, Y.; Zhao, L.; Jiao, Y.; Zhang, Y.; Jiang, Z.; Li, Q.; Wang, J.; Chen, S.; Yang, Y. Ag^{II} doped MIL-101 and its adsorption of iodine with high speed in solution. *J. Solid State Chem.* **2016**, *237*, 274−283.
(34) Yang, S. P.; Zhao, W.; Hu, P. P.; Wu, K. Y.; Jiang, Z. H.; Bai, L. P.; Li, M. M.; Chen, J. X. Lanthanum-based metal-organic frameworks for specific detection of Sudan virus RNA conservative sequences down to single-base mismatch. *Inorg. Chem.* **2017**, *56*, 14880−14887.
(35) Xie, B. P.; Qiu, G. H.; Hu, P. P.; Liang, Z.; Liang, Y. M.; Sun, B.; Bai, L. P.; Jiang, Z. H.; Chen, J. X. Simultaneous detection of Dengue and Zika virus RNA sequences with a three-dimensional Cu-based zwitterionic metal-organic framework, comparison of single and synchronous fluorescence analysis. *Sens. Actuators, B* **2018**, *254*, 1133−1140.
(36) Qiu, G. H.; Weng, Z. H.; Hu, P. P.; Duan, W. J.; Xie, B. P.; Sun, B.; Tang, X. Y.; Chen, J. X. Synchronous detection of ebolavirus conserved RNA sequences and ebolavirus-encoded miRNA-like fragment based on a zwitterionic copper (II) metal-organic framework. *Talanta* **2018**, *180*, 396−402.
(37) Zhao, H. Q.; Yang, S. P.; Ding, N. N.; Qin, L.; Qiu, G. H.; Chen, J. X.; Zhang, W. H.; Chen, W. H.; Hor, T. S. A zwitterionic 1D/2D polymer co-crystal and its polymorphic sub-components: a highly selective sensing platform for HIV ds-DNA sequences. *Dalton Trans.* **2016**, *45*, 5092−5100.
(38) Sheldrick, G. M. *SADABS: Program for empirical absorption correction of area detector data*; University of Göttingen: Göttingen, Germany, 1996.
(39) Sheldrick, G. M. *SHELXS-97 and SHELXL-97, programs for crystal structure solution and refinement*; University of Göttingen: Göttingen, Germany, 1997.
(40) Farrugia, L. J. WinGX suite for small-molecule single-crystal crystallography. *J. Appl. Crystallogr.* **1999**, *32*, 837−838.
(41) Spek, A. L. Single-crystal structure validation with the program PLATON. *J. Appl. Crystallogr.* **2003**, *36*, 7−13.
(42) *Molecular Operating Environment (MOE)*, 2014.09; Chemical Computing Group Inc.: Montreal, Quebec, Canada, 2014.
(43) Frisch, M. J.; Trucks, G. W.; Schlegel, H. B.; Scuseria, G. E.; Robb, M. A.; Cheeseman, J. R.; Scalmani, G.; Barone, V.; Mennucci, B.; Petersson, G. A.; Nakatsuji, H.; Caricato, M.; Li, X.; Hratchian, H. P.; Izmaylov, A. F.; Bloino, J.; Zheng, G.; Sonnenberg, J. L.; Hada, M.; Ehara, M.; Toyota, K.; Fukuda, R.; Hasegawa, J.; Ishida, M.; Nakajima, T.; Honda, Y.; Kitao, O.; Nakai, H.; Vreven, T.; Montgomery, J. A., Jr.; Peralta, J. E.; Ogliaro, F.; Bearpark, M.; Heyd, J. J.; Brothers, E.; Kudin, K. N.; Staroverov, V. N.; Kobayashi, R.; Normand, J.; Raghavachari, K.; Rendell, A.; Burant, J. C.; Iyengar, S. S.; Tomasi, J.; Cossi, M.; Rega, N.; Millam, J. M.; Klene, M.; Knox, J. E.; Cross, J. B.; Bakken, V.; Adamo, C.; Jaramillo, J.; Gomperts, R.; Stratmann, R. E.; Yazyev, O.; Austin, A. J.; Cammi, R.; Pomelli, C.; Ochterski, J. W.; Martin, R. L.; Morokuma, K.; Zakrzewski, V. G.; Voth, G. A.; Salvador, P.; Dannenberg, J. J.; Dapprich, S.; Daniels, A. D.; Farkas, O.; Foresman, J. B.; Ortiz, J. V.; Cioslowski, J.; Fox, D. J. *Gaussian 09*, revision D.01; Gaussian, Inc.: Wallingford, CT, 2009.
(44) *The PyMOL molecular graphics system*, version 1.8; Schrödinger, LLC, 2015.
(45) Yang, S. P.; Chen, S. R.; Liu, S. W.; Tang, X. Y.; Qin, L.; Qiu, G. H.; Chen, J. X.; Chen, W. H. Platforms formed from a three-dimensional Cu-based zwitterionic metal-organic framework and probe ss-DNA: selective fluorescent biosensors for human immunodeficiency virus 1 ds-DNA and Sudan virus RNA sequences. *Anal. Chem.* **2015**, *87*, 12206−12214.
(46) Qiu, G. H.; Lu, W. Z.; Hu, P. P.; Jiang, Z. H.; Bai, L. P.; Wang, T. R.; Li, M. M.; Chen, J. X. A metal-organic framework based PCR-

DOI: 10.1021/acs.inorgchem.8b01051
Inorg. Chem. XXXX, XXX, XXX−XXX

free biosensor for the detection of gastric cancer associated microRNAs. *J. Inorg. Biochem.* **2017**, *177*, 138−142.
(47) Sun, B.; Zhao, H. Q.; Xie, B. P.; Bai, L. P.; Jiang, Z. H.; Chen, J. X. Sequence-specific fluorometric recognition of HIV-1 ds-DNA with zwitterionic zinc(II)-carboxylate polymers. *J. Inorg. Biochem.* **2017**, *176*, 17−23.
(48) Zhao, H. Q.; Qiu, G. H.; Liang, Z.; Li, M. M.; Sun, B.; Qin, L.; Yang, S. P.; Chen, W. H.; Chen, J. X. A zinc(II)-based two-dimensional MOF for sensitive and selective sensing of HIV-1 ds-DNA sequences. *Anal. Chim. Acta* **2016**, *922*, 55−63.
(49) Qin, L.; Lin, L. X.; Fang, Z. P.; Yang, S. P.; Qiu, G. H.; Chen, J. X.; Chen, W. H. A water-stable metal-organic framework of a zwitterionic carboxylate with dysprosium: a sensing platform for Ebolavirus RNA sequences. *Chem. Commun.* **2016**, *52*, 132−135.
(50) Miyake, Y.; Togashi, H.; Tashiro, M.; Yamaguchi, H.; Oda, S.; Kudo, M.; Tanaka, Y.; Kondo, Y.; Sawa, R.; Fujimoto, T.; Machinami, T.; Ono, A. Mercury^{II}-mediated formation of thymine-Hg^{II}-thymine base pairs in DNA duplexes. *J. Am. Chem. Soc.* **2006**, *128*, 2172−2173.
(51) Ma, B.; Zeng, F.; Zheng, F.; Wu, S. A fluorescence turn-on sensor for iodide based on a thymine-Hg^{II}-thymine complex. *Chem. - Eur. J.* **2011**, *17*, 14844−14850.

DOI: 10.1021/acs.inorgchem.8b01051
Inorg. Chem. XXXX, XXX, XXX−XXX